ATMOSPHERIC RESPONSE TO OCEAN FRONTS AND EDDIES: A REVIEW

by

R. J. Small[1]

Acknowledging contributions from:

S. deSzoeke[1], **S. P. Xie**[1,2], **L. O'Neill**[3], **H. Seo**[4], **Q. Song**[3,5], **P. Cornillon**[5], **M. Spall**[6], **and S. Minobe**[7],

[1I]*nternational Pacific Research Center, University of Hawaii, Honolulu, HI*

[2] *Department of Meteorology, School of Ocean and Earth Science and Technology, University of Hawaii, Honolulu, HI.*

[3] *College of Oceanic and Atmospheric Sciences, Oregon State University, Corvallis, Oregon.*

[4] *Scripps Institution of Oceanography, La Jolla, California*

[5] *Graduate School of Oceanography, University of Rhode Island, Narragansett, Rhode Island*

[6] *Department of Physical Oceanography, Woods Hole Oceanographic Institution, Woods Hole, MA*

[7]*Earth and Planetary Sciences, Graduate School of Science, Hokkaido University, Sapporo, Japan*

Extended manuscript

for American Meteorology Society

Air-Sea Interaction Conference 2007

Abstract

Air-sea interaction at ocean fronts and eddies exhibits positive correlation between sea surface temperature (SST), wind speed, and heat fluxes out of the ocean, indicating that the ocean is forcing the atmosphere. This contrasts with larger scale climate modes where the negative correlations suggest that the atmosphere is driving the system. This paper reviews studies of the interaction of sharp SST gradients and the overlying marine atmospheric boundary layer and deeper atmosphere. The importance of different physical mechanisms of atmospheric response to SST gradients, such as the effect of surface stability variations on momentum transfer, pressure gradients, secondary circulations and cloud cover will be assessed. These processes will be compared and contrasted for different regions such as the Equatorial Front in the Eastern Pacific, and oceanic fronts in mid-latitudes such as the Gulf Stream, Kuroshio, and Agulhas Return Current.

1. Introduction

Recent observations of the nature of air-sea interaction over oceanic fronts and eddies have revealed a positive correlation of near-surface wind speed and SST (Chelton et al. 2001, Liu et al 2000, Hashizume et al 2001). This is a somewhat surprising result considering that on larger, basin scales, the correlation is often negative (Mantua et al. 1997; Okumura et al. 2001, Liu et al. 1994) which is interpreted as evidence that the atmosphere is driving an ocean response. In the large scale scenario, intensified winds cool the ocean surface through evaporation, as well as possibly increasing the entrainment of upper-thermocline cool waters into the mixed layer. The opposite type of response over the smaller ocean mesoscale features is suggestive of the ocean forcing the atmosphere, mainly through heat fluxes out of the ocean.

The global nature of air-sea interaction over ocean mesoscale features is illustrated in Figs. 1 and 2 using satellite data from the QuikSCAT scatterometer (launched in 1999), the Tropical Rainfall Measuring Mission (TRMM) Microwave Imager (TMI, launched in 1997), and the AQUA Advanced Scanning Microwave Radiometer for EOS (AMSR-E, launched in 2002). To reveal the scales of interest, filters are applied to the data. Typical ocean eddies have time periods of around 20-30 days at the equator (Tropical Instability Waves, Legeckis 1977, Lyman et al 2006) and 100s of days at mid-latitudes, and wavelengths ranging from ~1000 km at the equator (Legeckis 1977) to 100s of km in mid-latitudes (Stammer 1997), to 10s of kms in high latitudes (e.g. the Iceland-Fearoes front, Scott and McDowall 1990) and coastal zones, approximately following the latitude and stratification dependence of the internal baroclinic Rossby radius of deformation (see e.g. Chelton et al 1998, Killworth et al 1997). Therefore, filtering to remove spatial scales of 1000s of km or more, and temporal scales of a year or more, highlights the ocean mesoscale features and removes longer term modes such as El-Nino Southern Oscillation and Pacific Decadal Variability.

A map of the temporal correlation between high-pass[1] SST and neutral 10 m wind speed from TMI in the region equatorward of latitude 40° (Fig. 1) shows that positive correlation is dominant over most of the domain, reaching up to 0.6 in major frontal zones.[2] Using the shorter record length of AMSR-E, temporal averages of high pass data[3] over 2 months in boreal summer (Fig. 2) tell a similar story in mid and high latitudes: high pass filtered wind stress anomaly from QuikSCAT overlies anomalies of SST of the same sign. Here the SST anomalies are associated with the narrow jets and mesoscale eddies of the Kuroshio and its extension (Fig. 2a), the Gulf Stream and its extension, and the

[1] As the TRMM data is almost a decade long, the data is filtered temporally by removing the first three annual harmonics, and then applying a Fourier analysis and removing variability with time periods of around 40 weeks or more.
[2] Negative correlations of less than -0.2 are only found off Central America in association with gap-wind jets and upwelling (Trasvinas 1995), in the Gulf of Aden, and just north of the Mozambique channel.
[3] As the AMSR-E record is short (relative to TRMM), a spatial (Loess) filter has been applied instead, retaining spatial scales of approximately 10 degree latitude by 30 degree longitude or less.

North Atlantic Current (Fig. 2b), the Brazil-Malvinas confluence in the South Atlantic (Fig. 2c), and the Agulhas Current and Agulhas Return Current (Fig. 2d). The spatial correlation of the anomalous SST and wind stress computed from similar two-month mean maps range from 0.44 to 0.74 in these major frontal zones (Table 1).

There are several reasons why the atmosphere is affected by ocean fronts and eddies. i) Firstly, as air is blown across an SST gradient, an air-sea temperature difference and air-sea humidity difference is generated. This leads to changes in near-surface stability, and consequently the surface stress as well as latent and sensible heat fluxes (Sweet et al 1981, Businger and Shaw 1984, Hayes et al 1989). Changes in stability modify the well-known neutral logarithmic profiles within the surface layer such that the vertical gradients of wind velocity, air temperature and humidity are increased in stable conditions or decreased in unstable conditions (see e.g. Stull 1988). ii) The turbulent fluctuations of heat, moisture and momentum may be transported deeper into the boundary layer by large eddies, one result being a transfer of momentum from the upper boundary layer towards the surface (Hayes et al 1989, Wallace et al 1989). This will also lead to changes in the height of the boundary layer. iii) As the air temperature and moisture starts to respond to the surface fluxes, the atmospheric pressure also changes (Lindzen and Nigam 1987). This leads to a spatial pressure gradient which can drive secondary circulations (Wai and Stage 1989). iv) The surface currents of ocean fronts or eddies will either increase or reduce the relative motion of the air and ocean, acting to change the surface stress, thus affecting the atmosphere as well as feeding back onto the ocean (Kelly et al 2001, Cornillon and Park 2001).

In this paper, observations of the atmospheric response to ocean fronts will be described and compared for different oceanic regions. In section 2 three case studies are presented from equatorial and higher latitude regimes, and northern and southern hemispheres: the Equatorial Front in the Eastern Pacific, the Gulf Stream, and the Agulhas current/retroflection region. Section 3 contains a summary of

the observed atmospheric response, synthesizing the data from the case studies and other projects. Section 4 presents a Discussion. This paper is part of a larger project discussing the full air-sea interaction aspect (including the feedback onto the ocean) and containing theoretical and model results, which will be published in full in Dynamics of Atmospheres and Oceans (Small et al 2007).

2. Atmospheric Wind Response to Fronts and Eddies: Case studies from observations

The atmospheric response to SST distributions has been an area of long and rich study. Indeed Halley (1686) described the trade winds as the response to heating the air over the warmer ocean surface. Having lower density, the heated air rises, and is replaced by wind flowing from higher latitudes. This air gains an easterly component to conserve angular momentum (Hadley 1735). In the late 20th century the debate focused on how the atmospheric circulation responded to SST anomalies and gradients. Gill (1980) proposed a model of the tropical atmospheric circulation response to heating in the mid-troposphere. In this scenario convection anomalies drive low level wind anomalies and convergence. Although this model made no explicit reference to SST, subsequent papers added a simple dependence of heating on SST (Philander et al 1984, Hirst 1986, Gill and Rasmussen 1983). More sophisticated models then included the feedback effect of low level moisture flux convergence onto surface flux and hence heat anomaly (e.g. Zebiak 1986). An alternate model by Lindzen and Nigam (1987) related the circulation directly to the SST by hydrostatic pressure gradients induced in the marine atmospheric boundary layer (MABL). In their model surface winds near the equator (where the Coriolis parameter f is small) would consequently flow down the pressure gradient from cool SST to warm SST. The anomalous MABL wind field gradients then cause convergence of water vapor, leading to deep convection. Although it has been shown that the Gill model (as modified by Zebiak (1986) to include

SST) is mathematically similar to the Lindzen-Nigam model (Neelin 1989, Battisti et al 1999), the physics behind these models is different.

These models typically apply to large, basin-scale SST anomalies, to which the atmosphere has sufficiently large time to adjust, and are also appropriate for the tropics where the SST is high enough to initiate deep convection, such as in the warm pool regions. The processes which occur over mesoscale ocean SST anomalies, particular those occurring outside the warm pool, may be different than those that occur at basin scale. Due to the different densities of water and of air, mesoscale features such as fronts and eddies tend to be much smaller in the ocean, (on the scale of the first baroclinic Rossby radius, Chelton et al 1998) than in the atmosphere. For example high resolution ship surveys of the Equatorial Eastern Pacific front have determined that the temperature change occurs over less than 20 km (Yoder et al 1994), and close to Bermuda a 2°C change occurred over 100 m (Khalsa and Greenhut 1989), and ocean eddies typically have diameters on the order of 100 km in contrast to atmospheric pressure systems (1000 km). As a consequence, when the atmospheric wind blows across ocean fronts, it leads to rapid localised changes in the MABL.

One of the first intensive studies of air-sea interaction over fronts and eddies was the Joint Air-Sea Interaction (JASIN) experiment in the North Rockall Trough (59° N, 13° W) in the Atlantic in summer of 1978[4]. Businger and Shaw (1984) presented an analysis of the effect of ocean eddies on the atmospheric boundary layer using JASIN data and the Brown and Liu (1982) MABL model. During late summer of 1978, a cold atmospheric front passed a well instrumented array of moorings. The array measured a rapid increase in latent and sensible heat fluxes and wind stress as the cold air flowed from cool water towards an area of warm SST, in agreement with the predictions of the model. Businger and Shaw explained this with a conceptual model of MABL response to a warm eddy:

[4] (see e.g. 'Results of the Royal Society Joint Air-Sea Interaction project (JASIN)', Proceedings of a Royal Society discussion meeting held on 2 and 3 June 1982, ed. H Charnock and R T Pollard, pub Royal Society London 1983, also in Phil. Trans. R. Soc. Lon. A, 308, 221-429)

a) The boundary layer height increases in response to the larger turbulent heat fluxes, possibly leading to thicker stratocumulus where present.

b) A modest ‘heat-island effect’ or ‘land breeze’ occurs with winds flowing into the eddy.

c) The increased drag over the warmer water slows the wind over the eddy. Thus there is wind convergence on the upwind side and divergence on the downwind side. [Author’s note: this is the only part of the Businger and Shaw paper that appears to be directly refuted by later observations and models. In the results described below, it will be shown that although the drag increases over a warm eddy, the wind speed also increases. This leads to wind *divergence* on the upwind side and *convergence* on the downwind side].

d) The stress over the warm eddy increases as a result of the higher drag. For westerly winds this induces positive wind stress curl on the northern edge and negative curl on the southern edge.

These early findings (based on limited flight passes across an eddy) from JASIN and measurements across the Gulf Stream front by Sweet et al (1981) raised interest in performing more detailed analysis of the processes involved. In the following decades further intensive experiments such as the Frontal Air-Sea Interaction Experiment (FASINEX, Friehe et al 1991), the Genesis of Atlantic Lows Experiment (GALE, Dirks et al 1988), the Structure des Exchanges Mer-Atmosphère, Propriétés des Hétérogénéités Océaniques experiment (SEMAPHORE, Eymard 1998), and East Pacific Investigation of Climate Processes (EPIC, Raymond et al 2004), together with enhanced instrumentation on moorings such as Tropical-Atmosphere-Ocean (TAO), high resolution satellite data, and numerical models have been used to test these hypotheses. As will be seen below, some have stood the test of time whilst others have been refuted or modified.

In this section three regions are discussed in detail to describe, illustrate, and compare proposed mechanisms of MABL response to underlying SST gradients. The focus is on how the wind profile is

adjusted, as this is a question of much debate: but findings on the thermodynamic structure of the response are also discussed for completeness.

2.1 Equatorial front and Tropical Instability Waves

In the Eastern portions of the Pacific and Atlantic, equatorial upwelling driven by the Ekman divergence of trade winds creates a cold tongue of water for most of the year. These tongues are bordered by a sharp SST front to the north and a somewhat weaker front to the south (Fig. 3a shows a snapshot of the Pacific Equatorial Front). Meanders of the Equatorial Fronts, which have become known as Legeckis eddies or Tropical Instability Waves (TIWs: Dueing et al, 1975, Legeckis, 1977), are observed to grow in the east and propagate westwards (see Lyman et al, 2006, for a review). The unusual property of these fronts of being on or very close to the equator allow an examination of the air-sea interaction processes in the absence of strong effects of rotation.

In their seminal study of the surface winds over the Pacific cold tongue, Wallace et al (1989) showed from monthly mean US Comprehensive Ocean-Atmosphere Data Set (COADS) wind and SST fields that the SST frontal region was not the region of the strongest surface wind speed predicted by the Lindzen-Nigam model, but of the strongest surface wind divergence. Wallace et al (1989) formulated a mechanism to explain this discrepancy. They hypothesized that vertical transfer of momentum by mixing was adjusting the surface winds. In this explanation, over the stable conditions of the cold tongue, an upper level south-easterly wind jet is well-separated from weaker surface winds. The near surface air becomes more unstable when passing across the front towards warmer water, leading to enhanced mixing in the boundary layer, and momentum from the upper easterly jet is brought down to the surface, accelerating the surface wind.

In situ data from a single ship survey of the Equatorial Front at 125° W in September 1998 (Anderson 2001) confirmed the analysis of COADS data. In particular, an increase of 4° C across 2.5° latitude was found to coincide with an increase of meridional wind from 2 to 5ms^{-1}, and a change of sea-air temperature difference from 0.3° to 1.2° C. Meanwhile sea level pressure was reported to drop 2 hPa from the south side of the cold tongue to the far side of the north wall at 5° N.

The coupled air-sea system in the eastern tropical Pacific was the subject of more detailed investigation during the EPIC field experiment (Raymond et al 2004). The specific aims of EPIC included the investigation of convection in the Intertropical Convergence Zone (ITCZ), the dynamics of cross-equatorial flow, and the maintenance of the southeast Pacific tropical stratocumulus deck. As well as long period (3-4 years) enhanced monitoring at TAO moorings and in the south-east Pacific, the processes were surveyed in more detail in an intensive aircraft and ship campaign in September-October 2001.

As part of EPIC, eight aircraft missions measuring winds, temperature, humidity, turbulence, and turbulent fluxes were flown through the MABL along 95°W to investigate the nature of the cross-equatorial flow. Turbulent fluxes of heat and momentum were calculated from aircraft observations at 30 m (de Szoeke et al., 2005), which showed that the latent and sensible heat fluxes were nearly zero over the cold tongue, and 180 and 30 W m^{-2}, respectively, at 2° N. These large heat fluxes on the north side of the cold tongue were a source of buoyancy and mixing in the lower boundary layer, and contributed to MABL clouds and entrainment at the MABL top. Individual soundings (Fig. 4a) and the composited 95°W vertical cross-section (Fig. 4c) show that the atmospheric mixed layer increases with height as the front is crossed, as well as the boundary layer and inversion layer height. A wind jet at 500 m was observed over the equator above low surface wind speeds, whilst north of the cold tongue the mid-level jet appeared to descend towards the surface, with maximum near surface winds at around 3-4°

N (Fig. 4b, d). McGauley et al. (2004) found the strongest northward pressure gradient force at 2-3° N, due to the warmer boundary layer temperature on the north side of the SST front. Meridional surface stress also increased on the north side of the front, from 0.02 Pa at 0.8°S to 0.08 Pa at 0.6°N according to bulk measurements from the aircraft (deSzoeke et al 2005).

The atmospheric response to TIWs was first observed by Hayes et al. (1989) from early TAO measurements. By computing the meridional difference in wind velocity (e.g. from the equator to 2° N), they were able to isolate TIW induced fluctuations from large-scale, coherent wind structures. Hayes et al. found that there was a positive correlation between SST and southeasterly wind anomalies, with enhanced wind over the warm phase of TIWs. They attributed this to the momentum mixing mechanism of Wallace et al (1989). Xie et al (1998) utilised the broader coverage allowed by the European Remote Sensing (ERS) satellite scatterometer data and AVHRR SST data to produce spatial maps of TIWs and associated wind fields. By applying a high-pass spatial filter in the zonal direction they confirmed Hayes et al's (1989) findings obtained from the more limited in-situ data. These results were refined by the much better temporal sampling of the eddies obtained by the QuiKSCAT scatterometer[5] (Fig. 3b, c) as shown by Liu et al (2000), Chelton et al (2001), and Hashizume et al (2001). The relationship between SST and wind stress fields is seen more clearly in a spatial map of the one-point regressions of high pass filtered SST and wind vectors (Fig. 5a, modified from Hashizume et al 2001 and Small et al 2003). The amount of water vapor in the atmospheric column is enhanced over the TIW-induced wind convergence (Fig. 5c), associated with increased evaporation and moisture convergence. Cloud liquid water is enhanced over the warm SST (Fig. 5d). Ship-board soundings by Hashizume et al 2002 show that the MABL deepens over the warm phase of TIWs, favoring formation of stratocumulus clouds, as observed from satellite by Deser et al (1993).

[5] The ERS satellites cover 41% of the global ocean daily, compared with 93% for QuiKSCAT.

From measurements at TAO moorings, Thum et al (2002) showed that individual TIWs were associated with sensible and latent heat fluxes per °C of SST anomaly of around 4 W m^{-2} and 33 W m^{-2} (almost in phase with SST), respectively. These significant fluxes arise because the atmosphere is slow to respond to sharp SST gradients, leading to an air-sea temperature difference (Xie 2004). Cronin et al (2003) determined from enhanced TAO observations that the surface pressure responded by around 0.11hPa per °C, with the negative of the pressure (-*p*) leading the SST anomaly by around 4 days. As expected by hydrostatics, negative pressure anomalies were also found to be close in phase to air temperature. Advection by the mean easterlies shifted the air temperature and resultant hydrostatic pressure response downstream of the SST anomaly. Chelton et al (2001) investigated TIWs and found that positive wind stress curl was generated when the wind blew along the SST isotherms of the northern TIW front, due to the shear between the higher speeds to the right and lower speeds to the left of the air parcel (Fig. 3e). This led to an observed linear relationship between wind stress curl and crosswind component of SST gradient. Likewise wind stress divergence was linearly related to the alongwind component of SST gradient (Fig. 3d).

2.2 Gulf Stream and North Atlantic

In contrast to the Equatorial Front, which lies in an almost steady trade wind regime, western boundary currents (WBCs) and their associated SST gradients are often located in regions of variable winds, such as the mid-latitude storm tracks. Further, unlike the flow over the Equatorial front, flow over the WBCs will be influenced by the Earth's rotation. Therefore for comparative reasons it is useful to assess how the atmosphere responds to WBCs such as the Gulf Stream (discussed here), the Agulhas current (section 2.3) and the Kuroshio (see Nonaka and Xie 2003, White and Annis 2003), together with their more zonally aligned extensions.

The Gulf Stream is a strong poleward warm current in the western Atlantic with a large transfer of heat from the ocean to the atmosphere (see e.g. Tomczak and Godfrey 1994). During the late winter and early spring, the temperature is about 10°C warmer than the adjacent Continental Slope Water to the north. The associated large temperature gradient at the edge of the current produces significant atmospheric changes, which have often been noted by observers crossing the northern edge of the Gulf Stream. The Gulf Stream system can be considered in many ways to be an ideal experimental laboratory for observing frontal air-sea interaction processes.

Several in-situ experiments have studied the atmospheric response to the Gulf Stream and eddies. Sweet et al. (1981) reported changes in sea state, boundary layer winds and temperature across the front. The sea was rougher over the warm Gulf Stream, indicating a statically unstable interface. (A similar example of sea state change is illustrated in Fig. 6a.) In one flight, wind speed was greater (18-20 kt) and mixed layer deeper (914 m) over the Gulf Stream, compared to 8-10 kt and 600 m respectively over the slope water.

Analysis of the sea state variations seen in photographs such as Fig. 6a has been extended by various authors using spaceborne Synthetic Aperture Radar, which detects the cm to m scale waves on the sea surface. Weissman et al (1980) produced the first analysis of SAR imagery of the Gulf Stream and how it depended on the wind speed and SST. Sikora et al (1995) noted distinct surface roughness patterns either side of the Gulf Stream North Wall in one particular image (reproduced in Fig. 6b). On the east (warm) side, in unstable surface conditions, a ‘mottled’ surface pattern was taken to represent cellular convection, whereas over the cool SST to the west, a ‘marbled’ pattern with generally low backscatter and some curvilinear dark features was taken to represent low wind speed, stable conditions interspersed by oceanic frontal regions organizing surfactants into the linear features. Beal et al (1997) compiled a detailed intercomparison of SAR and AVHRR images which showed that the character of

the sea surface change across the Gulf Stream North Wall also depended on background wind direction. They interpreted the data in terms of a combined MABL model (based on Brown (1982)) and backscatter model using surface stability conditions measured from ship, which confirmed that step changes in backscatter were due to changes in stability. However they also noted that 'sea-breeze' effects, due to pressure gradients set up by thermal contrast across the front, were important.

It has long been known that besides their direct modification of the MABL, ocean fronts can influence synoptic storms. For instance, storm tracks measured in terms of cyclone frequency (Colucci 1977) or synoptic variability of surface stress (K. Kelly, pers. comm.) are located close to the Gulf Stream system. Indeed the rapid deepening of storms known as "Bombs" (defined as an extratropical surface cyclone with a surface pressure that falls on the average at least $1mbh^{-1}$ for 24 hours) has been observed to occur over the north flank of the Gulf Stream and Kuroshio (Sanders and Gyakum 1980, Sanders 1986, Cione et al 1993). Some of these intense synoptic or mesoscale storms can have unusual warm cores, related to a 'bent-back' warm front, more akin to tropical cyclones than typical extratropical lows (Neiman and Shapiro 1993, Businger et al 2005).

The response of synoptic storms to the Gulf Stream was investigated as part of GALE (Dirks et al 1988). The main focus of this large, multi-institution experiment was to study severe storms which typically develop off the East Coast of USA in winter and track northwards to later affect the north-eastern states. Cyclogenesis was found to be affected by offshore latent heat release and the appearance of coastal fronts. Air-sea temperature differences of up to 24°C were found to be associated with surface turbulent heat fluxes up to 1200 Wm^{-2} occurring in individual storms (Doyle and Warner 1990). Coastal atmospheric fronts were found to be typically aligned with either the Gulf Stream oceanic front or shelf fronts. Holt and Raman (1992) noted that the coastal front was a relatively shallow atmospheric front (less than 500 m deep) with higher clouds on the warm side of the front than over the cold side, where

clouds at 200 m lay above the internal boundary layer. Waves can develop along these coastal fronts and Holt and Raman (1992) and Doyle et al (1990) suggest that they can influence cyclogenesis, by providing a source of low level positive vorticity and moisture. In ideal conditions the combination of a baroclinic zone at the surface (surface temperature gradient) and a positive vorticity anomaly (or short wave trough) aloft is ideal for amplifying synoptic storms, as discussed in the framework of baroclinic instability theory by Hoskins et al (1985) and summarized in Holton (2004).

Recently, observations of Gulf Stream sea surface properties have been greatly enhanced due to the advent of microwave imaging satellite radiometers and satellite scatterometers such as QuiKSCAT, ERS and Adeos II. This has enabled the fine structure of the atmospheric response to the Gulf Stream to be detected, as shown by Chelton et al (2004) and Xie (2004). In particular it can be seen that there is a close co-location between extrema in 3-year mean SST seen from AMSR-E and extrema in the mean scalar 10 m neutral wind speed measured by QuiKSCAT (Fig. 7a), with the highest speeds (equivalently, largest stress magnitude) over warmer SST. The Gulf Stream also causes a signature in wind stress divergence and curl, the former being mostly due to acceleration of the winds which flow across the Gulf Stream in the mean (particularly north east of Cape Hatteras, Chelton et al 2004). The wind curl signature is partly due to the atmospheric response and partly due to the ocean currents, which may increase/decrease the stress when wind flows against/with the current (Kelly et al 2001, Chelton et al 2004).

The effect of the Gulf Stream on clouds has been studied by several authors. Young and Sikora (2003) performed a detailed analysis of the atmospheric mesoscale cloud formations which occurred when cold air flowing from the continent in winter behind synoptic storms is advected across the warm Gulf Stream. Many beautiful visible and infrared images showed mesoscale cloudbands forming on the upstream edge of the Gulf Stream north wall and trailing downstream (Young and Sikora 2003).

Sublette and Young (1996) documented a summer situation when background synoptic variability was weak and the SST gradients lead to a convergence zone, and boundary layer cloud, over the Gulf Stream. A map of the annual mean cloud liquid water in the North Atlantic from AMSR-E (Fig. 7b) shows a band of high liquid water content closely following the warm waters of the Gulf Stream and North Atlantic Current. Recent satellite observations of albedo from space also show a high correlation with underlying SST (Dudley Chelton, pers. comm.).

In addition to the Gulf Stream current, the response over the eddies shed by the Gulf Stream has also been analyzed. Recent studies by Cornillon and Park (2001), Park and Cornillon (2002), and Park et al. (2006) have demonstrated how ocean currents and changes in MABL stability associated with Gulf Stream rings affect the surface wind stress observed by scatterometers. In their study, the relationship between satellite-derived 10 m equivalent wind, U_{10}^{N}, and $T_{sea} - T_{air}$ in the vicinity of Gulf Stream rings was examined, using the sea surface temperature differences between water in the ring and water that surrounds it as a proxy for $T_{sea} - T_{air}$ (This assumes that the air is equilibriated to the ocean surface temperature outside the eddy, but does not have time to adjust its temperature when passing over the eddy. This is likely to overestimate the air-sea temperature difference as in reality the air will partially adjust to the eddy SST.) Park et al (2006) found that near-surface wind speeds increase by about 10% over warm core rings and reduced by around 15% over cold core rings (Fig. 8). Over warm core rings the strongest wind speeds are found over the core of the ring (Fig. 8a, b), consistent with boundary layer modification. Over cold core rings, the lowest speeds are found over and to the right of the core where the ocean current has a component in the same direction as the wind (Fig. 8c, d), so that the relative velocity is less than the wind speed: this suggests that the ocean currents are also modifying the measured stress. Over warm core rings there is strong divergence (convergence) on the upwind (downwind) side, while curl is strongly negative on the south edge of the ring boundary and positive on

the north edge. The opposite patterns are seen over cold core rings. An important effect of the enhanced convergence on the downwind side of warm core rings is seen in cloudiness fraction data from SST images, which reveals substantially enhanced cloud probabilities on the downwind side (Park et al. 2006).

2.3 Agulhas current/retroflection

Within 70km of the coast of South Africa, the Agulhas Current flows southwestward from the Indian Ocean before separating from the coast and turning abruptly along the southern tip of South Africa at the Agulhas Retroflection and continuing eastward as the Agulhas Return Current (Boebel et al. 2003a).

Several cyclonic and anti-cyclonic "Agulhas rings" and eddies are shed from the Agulhas Retroflection every year, each having a large surface expression that can persist several months as they propagate into the south Atlantic basin (Boebel et al. 2003b). Bathymetric-induced meanders along the Agulhas Return Current create alternating series of positive and negative SST perturbations in the SST front (Lutjeharms and van Ballegooyen 1984) that are generally quasi-stationary (at least during the period of the AMSR-E geophysical data record which commenced in June 2002, and confirmed in a longer record from drifters and altimetry by Parzan and Niiler (2004)). These features produce a rich array of small spatial scale (~100-1000 km) SST perturbations, which are illustrated in the 2 month mean map of spatially high-pass filtered SST from the AMSR-E in Fig. 2d. These features significantly influence the overlying marine atmospheric boundary layer as shown by the co-location of surface wind speed anomalies from QuikSCAT and the SST anomalies (Fig. 2d), and their high correlation (Table 1).

Spatial variations in wind speed associated with cross-frontal changes in SST produce perturbations in the wind stress curl and divergence field related to perturbations in the crosswind and

downwind SST gradients (Chelton et al. 2001; O'Neill et al. 2003, 2005; Chelton et al. 2004). These curl and divergence perturbations have a dynamic range nearly as large as the background large-scale curl and divergence fields (O'Neill et al. 2003).

Correlations between near surface winds and SST observed in satellite observations are consistent with limited in situ observations over the Agulhas Current and Agulhas Retroflection regions. Over the warm side of the Agulhas Current, surface latent and sensible heat fluxes increase dramatically (Jury and Walker 1988; Mey 1990: Jury 1994; Rouault and Lee-Thorp 1996; Rouault et al. 2000; Rouault and Lutjeharms 2000), with measurements indicating as much as a factor of 5 increase (Jury 1994). As winds blow from cool to warm water, increases in surface sensible and latent heat fluxes destabilize the boundary layer over the warmer water, enhancing vertical turbulent mixing, which deepens the boundary layer over the warmer water compared to cooler water. Boundary layer depth has been observed to change by as much as 300 m over the warmer water (Jury and Walker, 1988; Rouault et al. 2000). Cross-frontal boundary layer warming and deepening induces cross-frontal hydrostatic pressure perturbations, enhancing the cross-frontal surface flow from cooler to warmer water.

Observations over the Agulhas Current show that SST perturbations also affect low-level clouds. Cumulus and stratocumulus cloud decks are often seen to outline the position of the warmest waters of the Agulhas Current (Lutjeharms et al. 1986; Lee-Thorp et al. 1998; Lutjeharms and Rouault 2000) upstream of the Agulhas Retroflection region. From radiosonde and satellite observations during the Agulhas Current Air-Sea Exchange Experiment (ACASEX), Lee-Thorp et al. (1998) concluded that cumulus convection over the Agulhas Current was associated with decreases in boundary layer stability and increases in surface sensible and latent heat fluxes over warmer water. Analysis of columnar-integrated cloud liquid water (CLW) from AMSR-E in the Agulhas Return Current region, showed that anomalies of cloud liquid water of around $2x10^{-2}$ mm were located about 0.5° downwind of SST

anomalies. The magnitude of the anomalies could be explained by changes in stratocumulus thickness of a few hundred meters (O'Neill et al 2005).

From case studies and model sensitivity analyses, ocean-atmosphere interactions over the Agulhas Current have a significant impact on regional rainfall and storm intensity over southern Africa (e.g., Reason et al. 2001; Rouault et al. 2002; Singleton and Reason 2006). Large latent heat flux magnitudes over the core of the Agulhas Current enhance the precipitation over the southern portion of Africa (Rouault et al. 2002). In addition to supplying moisture to the overlying atmosphere, the SST structure of the Agulhas Current has been hypothesized to contribute to the location and intensity of a low-level wind jet, which funnels warm, moist air forming over the warmer waters of the Agulhas Current onshore (Singleton and Reason 2006).

3 Summary of MABL response to ocean fronts

The case studies described above, together with relevant studies of other regions, are used here to summarise the observed response of the MABL to ocean fronts.

3.1 Surface

Surface roughness and stress are modified across fronts, such that rougher water is typically observed over warm SST. In addition to the cases described above, changes in surface roughness across ocean fronts have also been observed in other regions of the World's Ocean: including in the Southern Ocean (Belkin and Romanov 1990), and in the Sargasso Sea (FASINEX: Friehe et al 1991). The increase in stress can be due to changes in surface stability and/or wind speed, and is observed globally by scatterometer (Chelton et al 2004) and by SAR (Sikora et al 1995). In all cases, wind stress curl (divergence) anomalies are linearly related to the component of the background wind across (along) the fine scale SST gradients (Chelton et al 2004).

3.2 Stratification and Cloud cover

Typically, stable or neutrally stable potential temperature profiles are observed over the cold side of fronts and unstable profiles over the warm side (e.g. in the eastern Equatorial Pacific), as might be expected from surface layer theory. These effects are actually felt much deeper in the boundary layer, and substantial changes in surface heat fluxes across fronts give rise to changes in boundary layer structure and height. Deepening of the boundary layer over warm water has been noted by several authors (include Kwon et al 1998, Sweet et al 1981, and Wayland and Raman 1989). This situation will be complicated in mid-latitude regions where the passage of synoptic atmospheric features such as cold-air outbreaks may play a more important role in setting the stratification over short time scales. Vihma et al (1991) noted that as well as synoptic events, the diurnal cycle also affects the near surface stability over oceanic fronts.

In some cases, a shallow internal boundary layer (IBL) is formed as air flows across a front. An IBL, which forms inside the pre-existing deeper boundary layer, can take the form of a shallow stable layer or unstable mixed layer depending on the sign of the air-sea temperature difference. This has been observed in the case of warm to cold water (Rogers 1989), where the IBL restricted the exchange of fluxes from surface to upper boundary layer. Also, for air flowing from cold to warm water, a shallow unstable IBL was observed to form across the Kuroshio by Hsu (1984b) and across the equatorial Front by Anderson (2001).

Warming and deepening of the boundary layer causes increased amounts of low-level cloudiness over the warm downwind side of SST fronts. Changes in cloud cover are observed, for instance in the warm sector of tropical instability waves (Deser et al 1993), and along the line of the Gulf Stream (Fig. 7b), and over the Agulhas Return Current. These clouds develop partly in response to the latent heat flux changes across the front, with turbulent eddies transporting moisture towards cooler air above, as well as

through organized ascent in secondary circulations. In the EPIC section across the Equatorial Front at 95° W, cloud-topped boundary layers (more precisely, stratocumulus and the occasional penetrating cumulus congestus) were found to be co-located with the region of maximum surface latent and sensible heat fluxes. Over the Gulf Stream, 'sea-smoke' rising from the seas surface has been observed and seen occasionally to link with particularly low cloud bases, presumably a sign of convective plumes (Wayland and Raman 1989). In contrast over the Cold Tongue, surface fog has been observed where warm moist air is advected across the cool surface (Nick Bond, pers. comm.). In FASINEX Rogers (1990) noted that surface forced clouds were present over warm water but over cold water the stable internal boundary layer inhibited the turbulent exchange between surface and cloud layer.

3.3 Wind profile

Changes of the surface wind due to SST were observed in situ and by satellites, but the perturbation to the wind extends much deeper, through the surface layer and the boundary layer. Observations over the eastern Equatorial Pacific show considerable wind shear over the cold water, and more uniform wind profiles over warm water, with the differences most marked over the lower 500 m (McGauley et al 2004, also Fig. 3).

In some observations notable jets form, within a few hundred meters of the surface, and these are referred to as low level jets (LLJs). LLJs are a common phenomenom in reasonably stable boundary layers over land, where they are related to baroclinicity (via the thermal wind equation) induced by weather systems, sloping terrain, and inertial oscillations (Stull 1988). (The LLJ over land often becomes stronger at night when turbulence reduces near the cold land surface, and momentum is not transferred to the surface but remains above in a nocturnal jet.) Similar jets have been observed near oceanic SST fronts. Vihma et al (1998) noted the presence of LLJs in 90% of rawinsonde soundings in a four week cruise at the Denmark Strait, which were most strong either when background flow was along

the front, so that the change in air temperature across the SST front enhanced the jet via thermal wind, or when warm air was advected over a cold surface (akin to the nocturnal jet case mentioned above), or when flow originated from the steep topography of Greenland (possibly due to the upstream orographic influence on baroclinicity also discussed above). Wayland and Raman (1989) detected a LLJ over the Gulf Stream at about 100 m height related to the baroclinic gradient.

In some observational studies the wind profile changes have been described as part of an ageostrophic secondary circulation. In SEMAPHORE, an experiment that took place close to the Azores Front in 1993 (Eymard 1998), considerable importance was given to the existence of ageostrophic winds as part of a thermally direct circulation cell. Marine boundary layer warming by surface sensible heat fluxes that arise from the SST change over a short distance appears to be the major contributor to the secondary circulation cell (Kwon et al 1998, Giordani et al 1998). In particular an increase of wind speed from the cold to the warm side of the front was attributed to these effects (Giordani et al 1998). Earlier Khalsa and Greenhut (1989) detected a secondary circulation induced by an SST front southwest of Bermuda in FASINEX.

4. Discussion.

The focus of this paper has been on air-sea interaction over mesoscale SST features, and its effect on the atmospheric boundary layer and the oceanic mixed layer. However, the response to the air-sea interaction is not just limited to the near-surface. In some regions of very large SST and SST gradients, observations have shown that the response can go well into the free troposphere. In situ observations of a rainband over the north wall of the Gulf Stream have been reported by Hobbs (1987) who termed it the ‘Gulf Stream Rainband’. This rainband can also be associated with rapidly developing

thunderstorms (Hobbs 1987, Trunk and Bosart 1990, Li et al 2004, Christian et al 2003), showing that the upper troposphere is also influenced by the SST[6].

The response of the extra-tropical atmosphere to large scale SST anomalies has produced many varied results in global AGCMs (Kushnir et al 2002), much of it related to the complexity of feedbacks between extratropical cyclones (referred to as storms here) and the mean flow. As a step towards solving this puzzle, it would be useful to understand how storms respond to smaller scale SST anomalies induced by ocean fronts and eddies. Mid-latitude storms typically grow through baroclinic instability and therefore require baroclinic sources (Chang et al 2002). One source is the low level (e.g. 850hPa to surface) temperature gradient, or baroclinicity (Hoskins and Valdes 1990) in the atmosphere, which in turn is related to the SST gradients (Cione et al 1993). Another source is diabatic heating which occurs when cold air in weather systems passes over the continental coasts and over ocean SST fronts as discussed in section 2.2. A full analysis of these effects should use new high resolution models and satellite data, current and upcoming experiments such as Kuroshio Extension Study (Tokinaga et al 2006), and the CLIVAR Mode Water Dynamics Experiment (CLIMODE, see www.climode.org) to compliment the findings from previous studies such as GALE.

The storm response to ocean fronts has been speculated to feed back onto the ocean and create a self sustaining system. Hoskins and Valdes (1990) showed that the storm-induced diabatic heating induces a steady circulation response which includes enhanced baroclinicity in the observed storm track entrance regions of the northern hemisphere. Further, they suggest that the strong mean and variable wind stress in the storm tracks is a major component of the atmospheric forcing of warm western boundary currents, which are essential ingredients for the diabatic heating. Nakamura and Shimpo (2004) also showed that the globally strongest wind stress, found in the Southern Indian Ocean,

[6] Further it has been noted that a maximum in mean upward vertical velocity at 300hPa from NCEP/NCAR reanalysis is closely co-located with the Gulf Stream (Minobe, pers. Comm..)

imparted by the transient atmospheric eddies, enhances the Antarctic Circumpolar Current SST front and hence the low level baroclinicity and the storm activity. This is another example of the importance of air-sea coupling over ocean fronts, as reviewed in Nakamura et al (2004).

Tropical cyclones and hurricanes can also be affected by SST gradients. As tropical cyclones require warm SST of greater than 26° C to fuel the latent heat release for growth (Emanuel 2003), this is to be expected. For instance Monaldo et al (1997: their Fig. 4) show a dramatic decrease in maximum wind of a hurricane as it crosses the Gulf Stream extension towards cooler water in mid-latitudes. Shay et al (2000) demonstrate that not just SST, but also heat content, are important in modifying hurricanes. As features such as the loop current in the Gulf of Mexico and the Gulf Stream are associated with changes in the mixed layer depth and thus heat content, they can be important factors in hurricane intensification as suggested for the recent hurricanes of the 2004 and 2005 season (e.g. Scharroo et al. 2005).

A major feedback onto the ocean is to be expected by extratropical storms or tropical cyclones modified by SST gradients (or heat content gradients). Bane and Osgood (1989) note the deepening of the mixed layer by about 35 m in the Gulf Stream due to a storm which was enhanced by Gulf-Stream-modified heat fluxes. Under the extreme winds of a hurricane, mixing and evaporative effects can leave a cool wake behind it as shown by e.g. Monaldo et al (1997), and this may affect primary production (Lin et al 2003). This process is most effective when the mixed layer is relatively shallow, and it may have some impact on subsequent tropical cyclogenesis.

The oceanic SST fronts discussed here cause rapid changes in the atmospheric MABL over scales of a few 100s of kms or much less. This has implications for atmospheric models and reanalyses which use SST as a boundary condition: the SST gradients need to be reasonably well resolved in order to get a sensible atmospheric response. For instance, Chelton (2005) has shown that the replacement of

the Reynolds SST (Reynolds et al 2002) in the ECMWF reanalysis model with that of the NOAA Real time global SST fields (RTG_SST) on a finer grid with less smoothing, lead to an improvement in the predicted surface stress fields. These improvements in turn will lead to improved ocean circulations predicted by ocean models forced by these stress fields. Coupled climate models are starting to approach the ability of ECMWF to represent the small scale SST/wind stress relationships, particularly for high resolution models such as MIROC (Hasumi and Emori 2004) (1.1 degree, T106) and the NCAR Community Climate System Model (CCSM3, Collins et al 2006) (1.4 deg., T85) (Maloney and Chelton, 2006)

References

Anderson, S. P., 2001. On the atmospheric boundary layer over the Equatorial Front. J. Clim., 14, 1688-1695.

Bane, J. M., and K. E. Osgood, 1989. Wintertime air-sea interaction processes across the Gulf Stream. J. Geophys. Res., 94, 10755-10772.

Battisti, D. S., E. S. Sarachik and A. C. Hirst, 1999. A consistent model for the large scale steady surface atmospheric circulation in the Tropics. J. Clim., 12, 2956-2964.

Beal, R. G., V. N. Kudryavtsev, D. R. Thomposon, S. A. Grodsky, D. G. Tilley, V. A. Dulov, and H. C. Graber, 1997. The influence of the marine atmospheric boundary layer on ERS 1 synthetic aperture radar imagery of the Gulf Stream. J. Geophys. Res., 102, 5799-5814.

Belkin, I.M and Y. A. Romanov, 1990. Surface currents and thermal fronts of the south Indian Ocean. Oceanology (English Translation), 30, 35-39.

Boebel, O., T. Rossby, J. R. E. Lutjeharms, W. Zenk, and C. Barron, 2003a. Path and variability of the Agulhas Return Current. Deep-Sea Res., 50:35-56.

Boebel, O., J. R. E. Lutjeharms, C. Schmid, W. Zenk, T. Rossby, and C. Barron, 2003b. The Cape Cauldorn: a regime of turbulent inter-ocean exchange. Deep-Sea Res., 50:57-86.

Brown, R. A., 1982. On two-layer models and the similarity functions for the PBL. Bound.-Layer Meteor., 24:451–463.

Brown, R. A., and W. T. Liu, 1982. An operational large scale marine PBL model. J. Applied. Meteorol., 21:261-269.

Businger, J. A. and W. J. Shaw, 1984. The response of the marine boundary layer to mesoscale variation in sea-surface temperature. Dynamics of Atmospheres and Oceans, 8:267–281.

Businger, S., T. M. Graziano, M. L. Kaplan and R. A. Rozumalski, 2005. Cold-air cyclogenesis along the Gulf Stream front: investigation of diabatic impacts on cyclone development, frontal structure and track. Meteorol. Atmos. Phys., 88, 65-90.

Chang, E. K. M., S. Lee and K. L. Swanson, 2002. Storm Track Dynamics. J. Climate, 15:2163-2183.

Chelton, D. B., 2005. The impact of SST specification on ECMWF surface wind stress fields in the Eastern Tropical Pacific. J. Clim., 18: 530-550.

Chelton, D. B., S. K. Esbensen, M. G. Schlax, N. Thum, M. H. Freilich, F. J. Wentz, C. L. Gentemann, M. J. McPhaden, and P. S. Schopf, 2001. Observations of coupling between surface wind stress and sea surface temperature in the eastern tropical Pacific. J. Climate, 14:1479-1498.

Chelton, D. B., M. H. Freilich, J. M. Sienkiewicz and J. M. VonAhn, 2006. On the Use of QuikSCAT scatterometer measurements of surface winds for Marine Weather Predictions. Mon. Wea. Rev., 134:2055-2071.

Chelton, D. B., M. G. Schlax, M. H. Freilich, and R. F. Milliff, 2004. Satellite measurements reveal persistent small-scale features in ocean winds. Science, 303, 978-983.

Chelton, D. B., M. G. Schlax, and R. M. Samelson, 2006.. Summertime coupling between sea surface temperature and wind stress in the California Current System. Submitted to J. Phys. Oceanogr.

Chelton, D. B., R. A. deSzoeke, M. G. Schlax, K. El Naggar and N Siwertz, 1998. Geographical variability of the first baroclinic Rossby radius of deformation. J. Phys. Oceanogr., 28, 433-460.

Christian, H. J., et al, 2003. Global frequency and distribution of lightning as observed from space by the Optical Transient Detector. J. Geophys. Res., 108, D1, 4005, doi 10.1029/2002JD002347.

Cione J. J., S. Raman, and L. J. Pietrafesa, 1993. The effect of Gulf Stream-induced baroclinicity on US East Coast winter cyclones. Mon. Wea. Rev., 121, 421-430.

Collins, W. D., C M. Bitz, M. L. Blackmon, G. B. Bonan, C. S. Bretherton, J. A. Carton, P. Chang, S. C. Doney, J. J. Hack, T. B. Henderson, J. T. Kiehl, W. G. Large, D. S. McKenna, B. D. Santer, and R. D. Smith. The Community Climate System Model Version 3 (CCSM3). J. Clim., 19, 2122–2143.

Colucci, S. J., 1977. Winter cyclone frequencies over the eastern United States and adjacent western Atlantic, 1964-1973. Bull. Am. Met. Soc., 57, 548-553.

Cornillon, P. and K.-A. Park, 2001. Warm core ring velocity inferred from NSCAT. Geophys. Res. Lett., 28, 575–578.

Cronin, M. F., S.-P. Xie, and H. Hashizume, 2003. Barometric pressure variations associated with eastern pacific tropical instability waves. J. Climate, 16, 3050–3057.

Deser, C, J. J. Bates, and S. Wahl, 1993. The influence of sea surface temperature on stratiform cloudiness along the equatorial front in the pacific Ocean. J. Clim., 6, 1172-1180.

Dirks, R. A., J. P. Kuettner, and J. A Moore, 1988. Genesis of Atlantic Lows Experiment (GALE): an overview. Bull. Am. Met. Soc., 69, 148-160.

Doyle, J. D., and T. T. Warner, 1990. Mesoscale coastal processes during GALE IOP 2, Mon. Wea. Rev., 118, 283-308.

Doyle, J. and T. Warner, 1992. The impact of the sea surface temperature resolution on mesoscale coastal processes during GALE IOP2. Mon. Wea. Rev., 121, 313–334.

Driedonks, A. G. M., 1982. Sensitivity analysis of the equations for a mixed layer. Bound. Lay. Met., 22, 475-480.

Düing, W., P. Hisard, E. Katz, J. Meincke, L. Miller, K. V. Moroshkin, G. Philander, A. A. Ribnikov, K. Voigt & R. Weisberg, 1975. Meanders and long waves in the equatorial Atlantic *Nature* 257, 280 – 284.

Emanuel, K, 2003. Tropical Cyclones. Annu. Rev. Earth Planet. Sci., 31, 75-104.

Eymard, L., 1998. The SEMAPHORE experiment. J. Geophys. Res., 103, 25005-25008.

Friehe C. A. et al, 1991.Air-sea fluxes and surface layer turbulence around a sea surface temperature front. J. Geophys. Res., 96, 8593-8609.

Gill, A. E., 1980. Some simple solutions for heat-induced tropical circulation. Quart. J. Roy. Met. Soc., 106, 447-462.

Gill, A. E., and E. M. Rasmussen, 1983. The 1982-83 climate anomaly in the equatorial Pacific. Nature, 306, 229-234.

Giordani, H, S. Planton, B. Benech and B.-H. Kwon, 1998. Atmospheric boundary layer response to sea surface temperatures during the SEMAPHORE experiment. J. Geophys. Res., 103, 25047-25060.

Hadley, G. 1735. concerning the cause of the general trade-winds. Phil. Trans., 39, 58-62.

Halley, E. 1686. An Historical Account of the Trade Winds, and Monsoons, observable in the Sea between and near the Tropicks, with an attempt to assign the Physical cause of the same winds, Phil. Trans.,16, 153-168.

Hashizume, H., S-P. Xie, W. T. Liu, and K. Takeuchi, 2001. Local and remote response to tropical instability waves: A global view from space. J. Geophys. Res., 106, 10173-10185.

Hashizume, H., Xie S-P., M. Fujiwara, M. Shiotani, T. Watanabe, Y. Tanimoto, W. T. Liu, and K. Takeuchi, 2002. Direct observations of inversion-capped boundary layer response to slow variations in sea surface temperature on the pacific Equatorial front. J. Climate, 15, 3379-3393.

Hasumi H., and S. Emori, ed., 2004. K-1 Coupled GCM (MIROC) description. K-1 Tech. Rep. No. 1.

Hayes, S. P., M. J. McPhaden and J. M. Wallace, 1989. The influence of sea surface temperature on surface wind in the eastern equatorial Pacific. weekly to monthly variability. J. Climate, 2, 1500-1506.

Hirst, A. C., 1986. Unstable and damped equatorial modes in simple coupled models. J. Atmos. Sci., 43, 606-630.

Hobbs, P. V., 1987. The Gulf Stream Rainband. Geophys. Res. Letts., 14, 1142-1145.

Holt, T. R., and S. Raman, 1992. Three-dimensional mean and turbulence structure of a coastal front influenced by the Gulf Stream. Mon. Wea. Rev., 120, 17-39.

Holton, J. R., 2004. An Introduction to Dynamical Meteorology. Fourth Edition, Elsevier Academic Press, 535pp.

Hoskins, B. J., M. E. McIntyre, and A. W. Robertson, 1985. On the use and significance of isentropic potential vorticity maps. Quart. J. Roy. Met. Soc., 111, 877-946.

Hoskins, B. J. and P. J. Valdes, 1990. On the existence of storm tracks. J. Atmos. Sci., 47, 1854-

1864.

Hsu, S. A., 1984. Effect of cold air advection on internal boundary-layer development over warm oceanic currents. Dyn. Atmos. Ocean., 8, 307-319.

Jury, M. R., 1994. A thermal front within the marine atmospheric boundary layer ove rthe Agulhas Current south of Africa: Composite aircraft observations. J. Geophys. Res., 99, 3297-3304.

Jury, M. R., and N. Walker, 1988. Marine boundary layer modification across the edge of the Agulhas Current. J. Geophys. Res., 93, 647-654.

Khalsa, S. J. S., and G. K. Greenhut, 1989. Atmospheric turbulence structure in the vicinity of an oceanic front. J. Geophys. Res., 94, 4913-4922.

Kwon, B.-H., B. Benech, D. Lambert, P. Durand, A. Druilhet, H. Giordani, and S. Planton, 1998. Structure of the marine atmospheric boundary layer over an oceanic thermal front: the SEMAPHORE experiment. J. Geophys. Res., 103, 25159-25180.

Lee-Thorp, A. M., M. Rouault, and J. R. E. Lutjeharms, 1998. Cumulus cloud formation above the Agulhas Current. S. Afr. J Sci., 94, 351-354.

Lee-Thorp, A. M., M. Rouault, and J. R. E. Lutjeharms, 1999. Moisture uptake in the boundary layer above the Agulhas Current: A case study. J. Geophy. Res., 104, 1423-1430.

Legeckis, R., 1977. Long waves in the eastern equatorial pacific Ocean: a view from a geostationary satellite. Science, 197, 1179-1181.

Li, X., W. Zheng, W. G. Pichel, C.-Z. Zou, P. Clemente-Colon, and K. S. Friedman, 2004: A cloud line over the Gulf Stream. Geophys. Res. Letts., 31, L14108, doi: 10.1029/2004GL019892.

Lin, I., W. T. Liu, C.-C. Wu, G. T. F. Wong, C. Hu, Z. Chen, W-D Liang, Y Yang and K.-K. Liu, 2003. New evidence for enhanced ocean primary production triggered by tropical cyclone. Geophys. Res. Letts., 30, doi: 10.1029/2003GL017141.

Lindzen, R. S. and S. Nigam, 1987. On the role of sea surface temperature gradients in forcing low level winds in the tropics. J. Atmos. Sci., 44, 2418-2436.

Liu, W. T, A. Zhang and J. K. B. Bishop, 1994. Evaporation and solar irradiance as regulators of sea surface temperature in annual and interannual change. J. Geophys. Res., 99, 12623-12637.

Liu, W. T., X. Xie, P. S. Polito, S.-P. Xie, and H. Hashizume, 2000. Atmospheric manifestation of tropical instability waves observed by QuikSCAT and Tropical Rain Measuring Mission. Geophys. Res. Letts., 27, 2545-2548.

Lutjeharms, J. R. E., and R. C. van Ballegooyen, 1984. Topographic control in the Agulhas Current System. Deep-Sea Res., 31, 1321-1337.

Lutjeharms, J. R. E., R. D. Mev, and I. E. Hunter, 1986. Cloud lines over the Agulhas Current. S. Afr. J. Sci., 82, 635-640.

Lutjeharms, J. R. E., and M. Rouault, 2000. Observations of cloud formation above Agulhas Current intrusions in the southeast Atlantic. S. Afr. J. Sci., 96, 577-580.

Lyman, J. M., G. C. Johnson and W. S. Kessler, 2006. Distinct 17 day and 33 day Tropical Instability Waves in subsurface observations. J. Phys. Oceanogr., in press.

McGauley, M., C. Zhang and N. A. Bond, 2004. Large-scale characteristics of the Atmospheric Boundary layer in the Eastern pacific cold tongue/ITCZ region. J. Climate, 17, 3907-3920.

Maloney, E. D., and D. B. Chelton, 2006. An assessment of the sea surface temperature influence on surface wind stress in numerical weather prediction and climate models. J. Clim., 19, 2743-2762.

Mantua, N. J., S. R. Hare, Y. Zhang, J. M. Wallace, and R. C. Francis, 1997. A Pacific interdecadal climate oscillation with impacts on salmon production. Bull. Am. Met. Soc., 78, 1069-1079.

Mey, R. D., N. D. Walker, and M. R. Jury, 1990: Surface heat fluxes and marine boundary layer modification in the Agulhas Retroflection region. J. Geophys. Res., 95, 15997-16015.

Monaldo F. M., T. D. Sikora, S. M. Babin and R. E. Sterner, 1997. Satellite imagery of sea surface temperature cooling in the wake of Hurricane Edouard. Mon. Wea. Rev., 125, 2716-2721.

Nakamura H., T. Sampe, Y. Tanimoto and A. Shimpo, 2004. Observed associations along Storm Tracks, Jet Streams and mid-latitude Oceanic Fronts. Earth's Climate: the Ocean-Atmosphere interaction, pp329-345. Geophysical Monograph Series 147, pub. Am. Geophys. Union..

Nakamura H., and A. Shimpo, 2004. Seasonal variations in the Southern Hemisphere Storm Tracks and jet Streams as Revealed in a Reanalysis dataset. J. Climate, 17, 1828-1844.

Neelin, J. D., 1989. On the interpretation of the Gill model. J. Atmos. Sci., 46, 2466-2468.

Neiman, P. J., and M. A. Shapiro, 1993. The life cycle of an extratropical marine cyclone. Part 1: Frontal-cyclone evolution and thermodynamic air-sea interaction. Mon. Wea. Rev., 121, 2153-2176.

Ohfuchi, W., H. Sasaki., Y. Masumoto and H. Nakamura, 2005 "Mesoscale resolving simulations of the Global Atmosphere and Ocean on the earth Simulator. EOS Trans. Am. Geophys. Union, 86, 45-46.,

Okumura, Y., S.-P. Xie, A. Numaguti and Y. Tanimoto, 2001. Tropical Atlantic air-sea interaction and its influence on the NAO. Geophys. Res. Letts., 28, 1507-1510.

O'Neill, L. W., D. B. Chelton, and S. K. Esbensen, 2003. Observations of SST-induced perturbations of the wind stress field over the Southern Ocean on seasonal time scales. J. Climate, 16, 2340-2354.

O'Neill, L. W., D. B. Chelton, S. K. Esbensen, and F. J. Wentz, 2005. High-resolution satellite measurements of the atmospheric boundary layer response to SST variations along the Agulhas Return Current. J. Clim., 18, 2706-2723.

Nonaka, M. and S.-P. Xie, 2003. Covariations of sea surface temperature and wind over the Kuroshio and its extension: evidence for ocean to atmosphere feedback. J. Climate, 16, 1404-1413.

Park, K.-A. and P. Cornillon, 2002. Stability-induced modification of sea surface winds over Gulf Stream rings. Geophys. Res. Lett., 29, 2211–2214.

Park, K.-A., P. Cornillon, and D. L. Codiga, 2006. Modification of surface winds near ocean fronts: Effects of Gulf Stream rings on scatterometer (QuikSCAT, NSCAT) wind observations. J. Geophys. Res., 111, C03021, doi:10.1029/2005JC003016.

Pazan, S. E. and P. Niiler, 2004. Ocean Sciences: New Global Drifter Data Set Available EOS, Trans. Am. Geophys. Union, 85, 2, 17.

Philander, S. G., T. Yamagata, and R. C. Paicanowski, 1984. Unstable air–sea interaction in the Tropics. J. Atmos. Sci., **41,** 604–613.

Polito, P. S.,J. P. Ryan, W. T. Liu and F. P. Chavez, 2001. Oceanic and atmospheric anomalies of Tropical Instability Waves. Geophys. Res. Letts., 28, 2233-2236.

Raymond D. J., S.K. Esbensen, M. Gregg, C. S. Bretherton, L. K. Shay, T. Uttal, and P. Zuidema, 2004. EPIC2001 and the coupled ocean-atmosphere system of the tropical east Pacific, Bull. Amer. Meteor. Soc., 85, 1341-1354.

Reason, C. J. C., 2001: Evidence for the influence of the Agulhas Current on regional atmospheric circulation patterns. J. Climate, 14, 2769-2778.

Reynolds, R. W., N. A. Rayner, T. M. Smith, D. C. Stokes and W. Wang, 2002. An improved in situ and satellite SST analysis for climate. J. Climate, 15, 1609-1625.

Rogers, D. P., 1989. The marine boundary layer in the vicinity of an ocean front. J. Atmos. Sci., 46, 2044-2062.

Rouault, M., and A. M. Lee-Thorp, 1996. Fine-time resolution measurements of atmospheric boundary layer properties between Cape Town and Marion Island. S. Afr. J. Mar. Sci., 17, 281-296.

Rouault, M., and J. R. E. Lutjeharms, 2000. Air-sea exchange over an Agulhas eddy at the subtropical convergence. Global Atmos. Ocean Syst., 7, 125-150.

Rouault, M., A. M. Lee-Thorp, and J. R. E. Lutjeharms, 2000. The atmospheric boundary layer above the Agulhas Current during Alongcurrent winds. J. Phys. Ocean., 30, 40-50.

Rouault, M., C. J. C. Reason, J. R. E. Lutjeharms and A. C. M. Beljaars, 2003. Underestimation of latent and sensible heat fluxes above the Agulhas Current in NCEP and ECMWF analyses. J.Clim.,16, 776-782.

Sanders, F., 1986. Explosive cyclogenesis in the west-central North Atlantic Ocean, 1981-1984. Part I: composite structure and mean behavior. Mon. Wea. Rev., 114, 1781-1794.

Sanders and Gyakum, 1980. Synoptic-Dynamic climatology of the “Bomb”. Mon. Wea. Rev., 108, 1589-1606.

Scharroo, R., N. H. Cornish, W. H. F. Smith and J. L. Lillibridge, 2005. Satellite altimetry and the intensification of Hurricane Katrina. EOS Trans. Am. Geophys. Un., 86, 366.

Scott, J. C. and A. L. McDowall, 1990. Cross-frontal cold jets near Iceland: in-water, satellite infrared and Geosat altimeter data. J. Geophys. Res., 95, 18005-18014.

Seo, H., A. J. Miller and J. O. Roads, 2007a. The Scripps Coupled Ocean-Atmosphere Regional (SCOAR) model, with applications in the Eastern Pacific Center. Journal of Climate, 20, 381-402

Shay, L. K., G. J. Goni and P. G. Black, 2000. Effects of a warm oceanic feature on Hurricane Opal. Mon. Wea. Rev., 128, 1366-1383.

Sikora, T. D., G. S. Young, R. C. Beal, and J. D. Edson, 1995. Use of spaceborne synthetic aperture radar of the sea surface in detecting the presence and structure of the convective marine atmospheric boundary layer. Mon. Wea. Rev., 123, 3623-3632.

Singleton, A. T., and C. J. C. Reason, 2006: Numerical studies of a severe rainfall event over the Eastern Cape coast of South Africa: sensitivity to sea surface temperature and topography. Tellus, 58A, 355-367.

Small J., Xie S-P and Y. Wang, 2003. 'Numerical simulation of atmospheric response to Tropical Instability Waves', J. Climate, 16, 3722-3740.

Small R. J., Xie S-P., and J. Hafner, 2005. 'Satellite observations of mesoscale ocean features and co-propagating atmospheric surface fields in the Tropical belt', J. Geophys. Res, 110, doi:10.1029/2004JC002598.

Small, R. J., S. P. DeSzoeke, S. P. Xie, L. O'Neill, H. Seo, Q. Song, P. Cornillon, M. Spall and S. Minobe, 2007: 'Air-sea interaction over ocean fronts and eddies', accepted, Dyn. Atmos. Ocean.. Available at http://iprc.soest.hawaii.edu/~justins/

Stammer, D. (1997), Global characteristics of ocean variability estimated from regional TOPEX/POSEIDON altimeter measurements. *J. Phys. Oceanogr*., *27*, 1743-1769.

Stull, R. B., 1988: An introduction to boundary layer meteorology. Kluwer Academic Publishers, Dordrecht, NL, 666 pp.

Sublette, M. S. and G. S. Young, 1996. Warm-season effects of the Gulf Stream on mesoscale characteristics of the atmospheric boundary layer. Mon.Wea. Rev., 124, 653-667.

Sweet, W., R. Fett, J. Kerling, and P. LaViolette, 1981. Air-sea interaction effects in the lower troposphere across the north wall of the Gulf Stream. Mon.Wea. Rev., 109, 1042–1052.

de Szoeke, S. P., C. S.Bretherton, N. A.Bond, M. F.Cronin, and B. M.Morley, 2005. EPIC 95°W Observations of the Eastern Pacific Atmospheric Boundary Layer from the Cold Tongue to the ITCZ. J. Atmos. Sci., 62, 426-442

Thum, N., S. K. Esbensen, D. B. Chelton and M. J. McPhaden, 2002. Air-sea heat exchange along the northern sea surface temperature front in the eastern tropical Pacific. J Climate, 15, 3361-3378.

Tokinaga, H., Y. Tanimoto, M. Nonaka, B. Taguchi, T. Fukamachi, S.-P. Xie, H. Nakamura, T. Watanabe and I. Yasuda, 2006. Atmospheric sounding over the winter Kuroshio Extension: effect of surface stability on atmospheric boundary layer structure. Geophys. Res. Letts., 33, L04703, doi: 10.1029/2005GL025102.

Tomczak, M. and J. S Godfrey, 1994. Regional Oceanography: an Introduction. Pergamon, 422pp.

Trunk, T. J., and L. F. Bosart, 1990. Mean radar echo characteristics during project GALE. Mon. Wea. Rev., 118, 459-469.

Vihma, T., J. Launiainen and G. Krause, 1991. On the air-sea interaction in areas of thermal marine fronts in the Greenland Sea. Atmos. Ocean., 29, 596-610.

Vihma, T., J. Uotila and J. Launiainen, 1998. Air-sea interaction over a thermal marine front in the Denmark Strait. J. Geophys. Res., 103, 27665-27678.

Wai, M. M. and S. A. Stage, 1989. Dynamical analyses of marine atmospheric boundary layer structure near the Gulf Stream oceanic front. Quart. J. Roy. Meteor. Soc., 115, 29–44.

Wallace, J. M., T. P. Mitchell and C. Deser, 1989. The influence of Sea Surface Temperature on surface wind in the eastern equatorial Pacific: seasonal and interannual variability. J. Climate, 2, 1492-1499.

Wayland, R. J., and S. Raman, 1989. Mean and turbulent structure of a baroclinic marine boundary layer during the 28 January 1986 cold air outbreak (GALE 1986). Bound. Lay. Met., 48, 227-254.

Weissman, D. E., T. W. Thompson, and R. Legeckis, 1980. Modulation of sea surface cross section by surface stress: wind speed and temperature effects across the Gulf Stream. J. Geophys. Res., 85, 5032-5042.

White, W. B. and J. L. Annis 2003. Coupling of extratropical mesoscale eddies in the ocean to westerly winds in the atmospheric boundary layer. J. Phys. Oceanogr., 33, 1095-1107.

Xie, S-P., M. Ishiwatari, H. Hashizume, and K. Takeuchi, 1998. Coupled ocean-atmospheric waves on the equatorial front. Geophys. Res. Letts., 25, 3863-3866.

Xie, S.-P. 2004. Satellite observations of cool ocean-atmosphere interaction. Bull. Amer. Meteor. Soc., 85, 195-208.

Yoder, J. A., S. G. Ackleson, R. T. Barber, P. Flament and W. M. Balch, 1994. A line in the sea. Nature, 371, 689-692.

Young, G. S. and T. D. Sikora, 2003. Mesoscale stratocumulus bands caused by Gulf Stream Meanders. Mon. Wea. Rev., 131, 2177-2191.

Zebiak, S. E., 1986. Atmospheric convergence feedback in a simple model for El-Nino. Mon. Wea. Rev., 114, 1263-1271.

Correlations by Region	Jan.-Feb. 2003	Jul-Aug 2003
Kuroshio 30° to 55° N, 120°E to 160° W	0.440	0.438
Gulf Stream35° to 60° N, 80°W to 15° W	0.569	0.568
South Atlantic 30° to 60° S, 70°W to 25° W	0.645	0.742
Agulhas 30° to 60° S, 0° to 100° E	0.631	0.649
Global	**0.39**	**0.42**

Table 1. Correlation coefficients computed from the spatial map of high pass filtered SST and wind stress magnitude shown in Fig. 2. The coefficients are given for the four defined regions and for a near-global domain (from 70°S to 70° N), and for boreal winter and summer 2003.

Figure Captions.

Figure 1. A map of the correlation of SST and neutral 10m wind speed, both pre-filtered to emphasise meso-scale features. The mean SST (interval 3K) is overlaid. Data from TRMM, 1997-2004. The data was filtered as follows: the first three annual harmonics were first removed, then a Fourier filter has been applied to retain only features of around 40 week period or less.

Figure 2. Maps of spatially high pass filtered 2 month (May-June 2003) average wind stress magnitude(color) and SST (°C, contours, interval 0.5°C, zero contour omitted). Data from QuikSCAT scatterometer and AMSR-E. a) North-west Pacific, Kuroshio region b) North-west Atlantic, Gulf Stream and North Atlantic Current region c) South-west Atlantic, Brazil-Malvinas confluence, and d) Southern Indian Ocean, Agulhas Return Current.

Figure 3. Three-day average maps over the period 2-4 September 1999 showing Tropical Instability Waves: (a) sea surface temperature with TAO mooring locations shown as squares; (b) wind stress magnitude; (c) wind stress; (d) wind stress divergence; and (e) wind stress curl. The contours overlaid in (b)-(e) correspond to isotherms at intervals of 1°C between 21° and 27°C. From Chelton et al (2001). Reproduced by permission of the American Meteorological Society.

Figure 4. EPIC 2001 observations of the MABL across the Equatorial Front at 95° W. Potential temperature (a) and meridional velocity (b) from representative dropwinsoundes in the cold tongue (dot-dash) and north of the front (solid). C), d) Cross-section composited from in situ data from 8 flights by the NCAR C-130 aircraft. Adapted from deSzoeke et al. (2005) by permission of the American Meteorological Society.

Figure 5. Composite regression onto SST at a center point of 120° W, 2° N. a) Observed SST (color) and wind velocity ($ms^{-1}K^{-1}$, see scale arrow) and wind speed($ms^{-1}K^{-1}$,

contours, 0.1 $ms^{-1}K^{-1}$,interval), b) Model wind velocity ($ms^{-1}K^{-1}$, see scale arrow) and wind speed($ms^{-1}K^{-1}$, contours, 0.1 $ms^{-1}K^{-1}$,interval) forced by observed SST (color) at the surface, c) Water vapor (color, mmK^{-1}), SST (black contoured at 0.1 intervals) and wind convergence ($s^{-1}K^{-1}$, white contours, contoured for +/- 1,2,3x10^{-6} $s^{-1}K^{-1}$), d) cloud liquid water (color, $10^{-3}mmK^{-1}$) and SST (contoured at 0.1 intervals). Adapted from Small et al (2003) by permission of the American Meteorological Society.

Figure 6. a) Photograph taken from the NOAA P-3 aircraft looking northeast across the north wall of the Gulf Stream. The winds were blowing from the northeast at the time of the photograph. The seas were calm over the colder waters to the northwest of the Gulf Stream (upper left) and white caps covered the warmer water to the southeast. (Courtesy of P. Chang and D. Chelton). From Chelton et al (2006). Reproduced by permission of American Meteorological Society. b) SAR image showing convective cells over Gulf Stream water (bottom right): smooth waters over cool shelf water (top left). From Sikora et al 1995. Reproduced by permission of the American Meteorological Society.

Figure 7. a. North-west Atlantic SST (color, °C) and mean neutral 10 m wind speed (ms^{-1}, 1 ms^{-1} contour interval), and vectors (see scale at bottom right). A 3 year mean from June 2002 to June 2005. SST from AMSR-E and winds from QuiKSCAT. B) column integrated cloud liquid water (10^{-1} mm, color) and SST (contours at 3°C intervals). A 3 year mean from June 2002 to June 2005 from AMSR-E.

Figure 8. Gulf Stream rings. Component of scatterometer winds along the mean wind direction, in ring-centric coordinates rotated such that the mean wind is towards the top of the figure. data are binned by mean wind speed, data set, and type of ring and averaged over all rings. A) warm core rings from QSCAT, b) warm core rings from NSCAT, c) cold core rings

from QSCAT, d) cold core rings from NSCAT. From Park et al (2006). Copyright American Geophysical Union (2006) and reproduced by their permission.

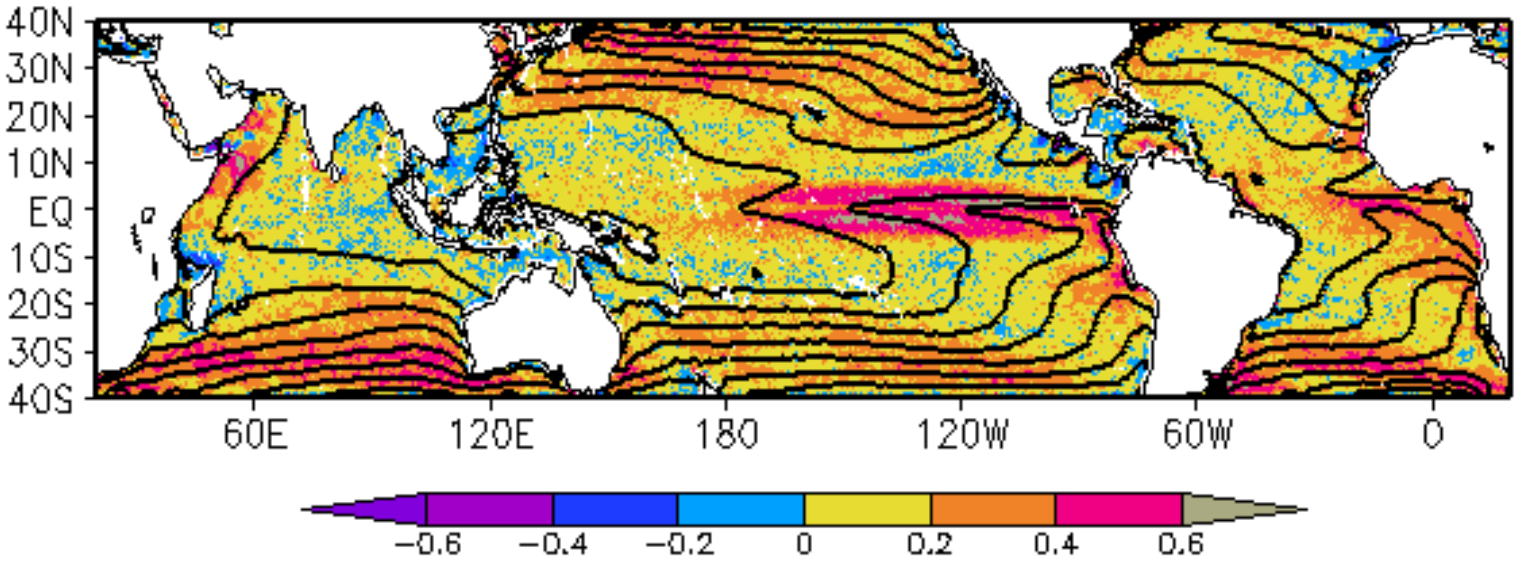

Figure 1. A map of the correlation of SST and neutral 10m wind speed, both pre-filtered to emphasise meso-scale features. The mean SST (interval 3K) is overlaid. Data from TRMM, 1997-2004. The data was filtered as follows: the first three annual harmonics were first removed, then a Fourier filter has been applied to retain only features of around 40 week period or less.

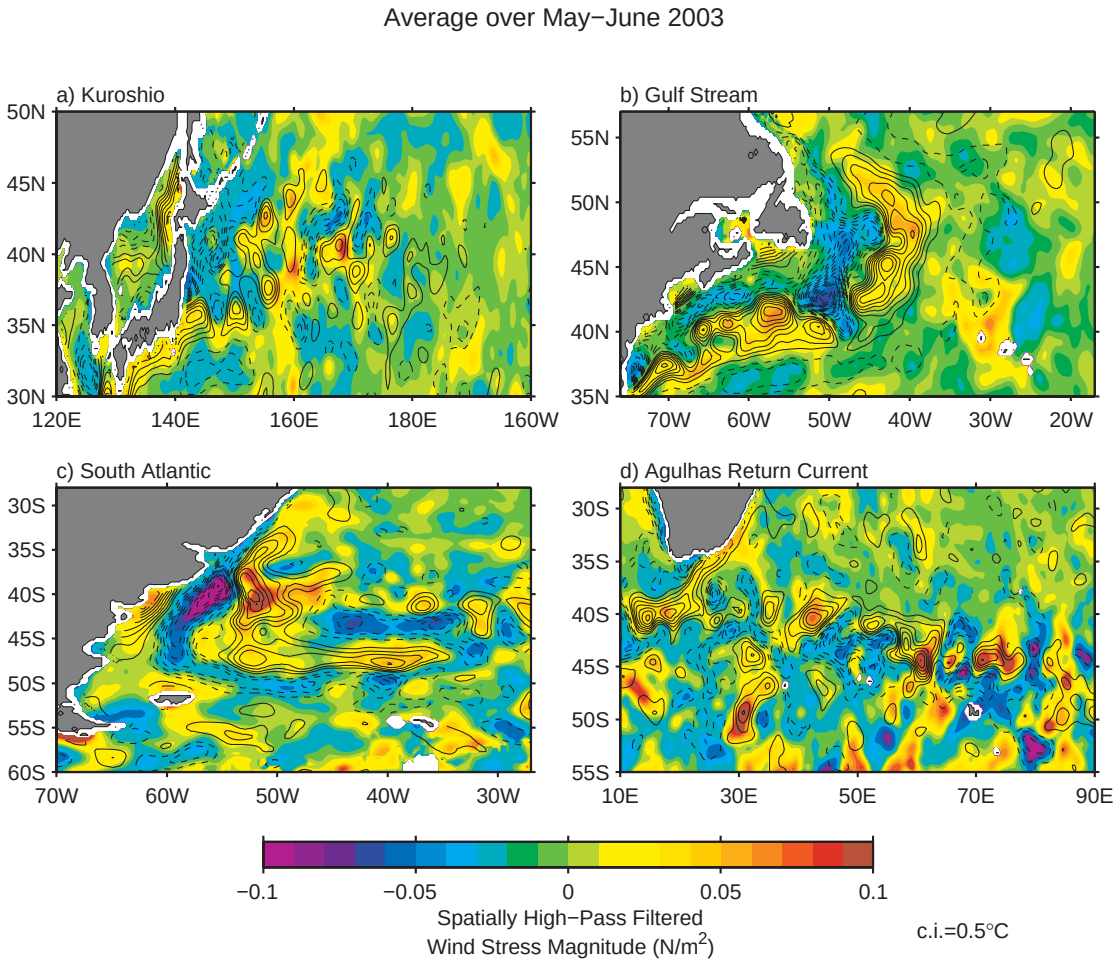

Figure 2. Maps of spatially high pass filtered 2 month (May-June 2003) average wind stress magnitude(color) and SST (°C, contours, interval 0.5°C, zero contour omitted). Data from QuikSCAT scatterometer and AMSR-E. a) North-west Pacific, Kuroshio region b) North-west Atlantic, Gulf Stream and North Atlantic Current region c) South-west Atlantic, Brazil-Malvinas confluence, and d) Southern Indian Ocean, Agulhas Return Current.

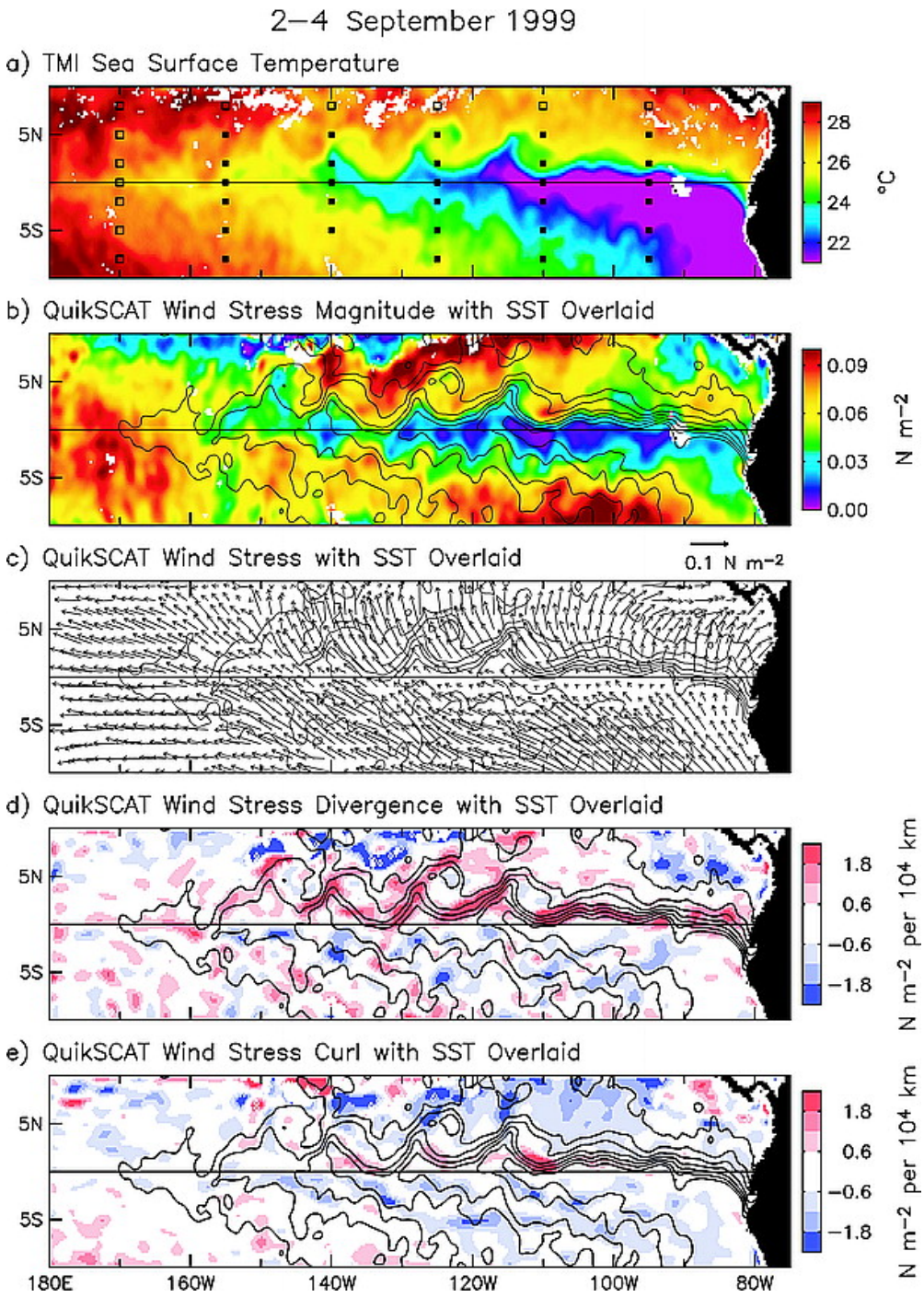

Fig. 3. Three-day average maps over the period 2-4 September 1999 showing Tropical Instability Waves: (a) sea surface temperature with TAO mooring locations shown as squares; (b) wind stress magnitude; (c) wind stress; (d) wind stress divergence; and (e) wind stress curl. The contours overlaid in (b)-(e) correspond to isotherms at intervals of 1°C between 21° and 27°C. From Chelton et al (2001). Reproduced by permission of the American Meteorological Society.

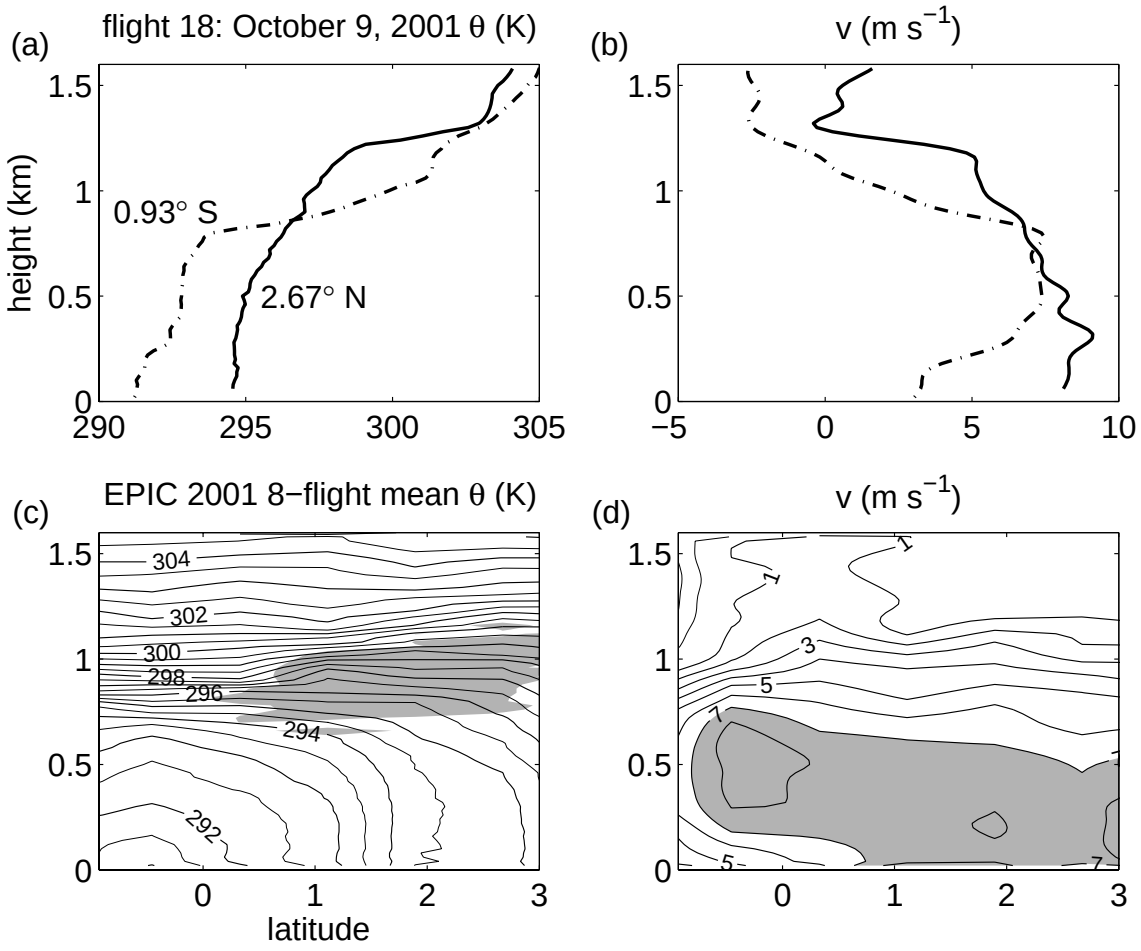

Figure 4. EPIC 2001 observations of the MABL across the Equatorial Front at 95° W. Potential temperature (a) and meridional velocity (b) from representative dropwinsoundes in the cold tongue (dot-dash) and north of the front (solid). C), d) Cross-section composited from in situ data from 8 flights by the NCAR C-130 aircraft. Adapted from deSzoeke et al. (2005) with permission of the American Meteorological Society.

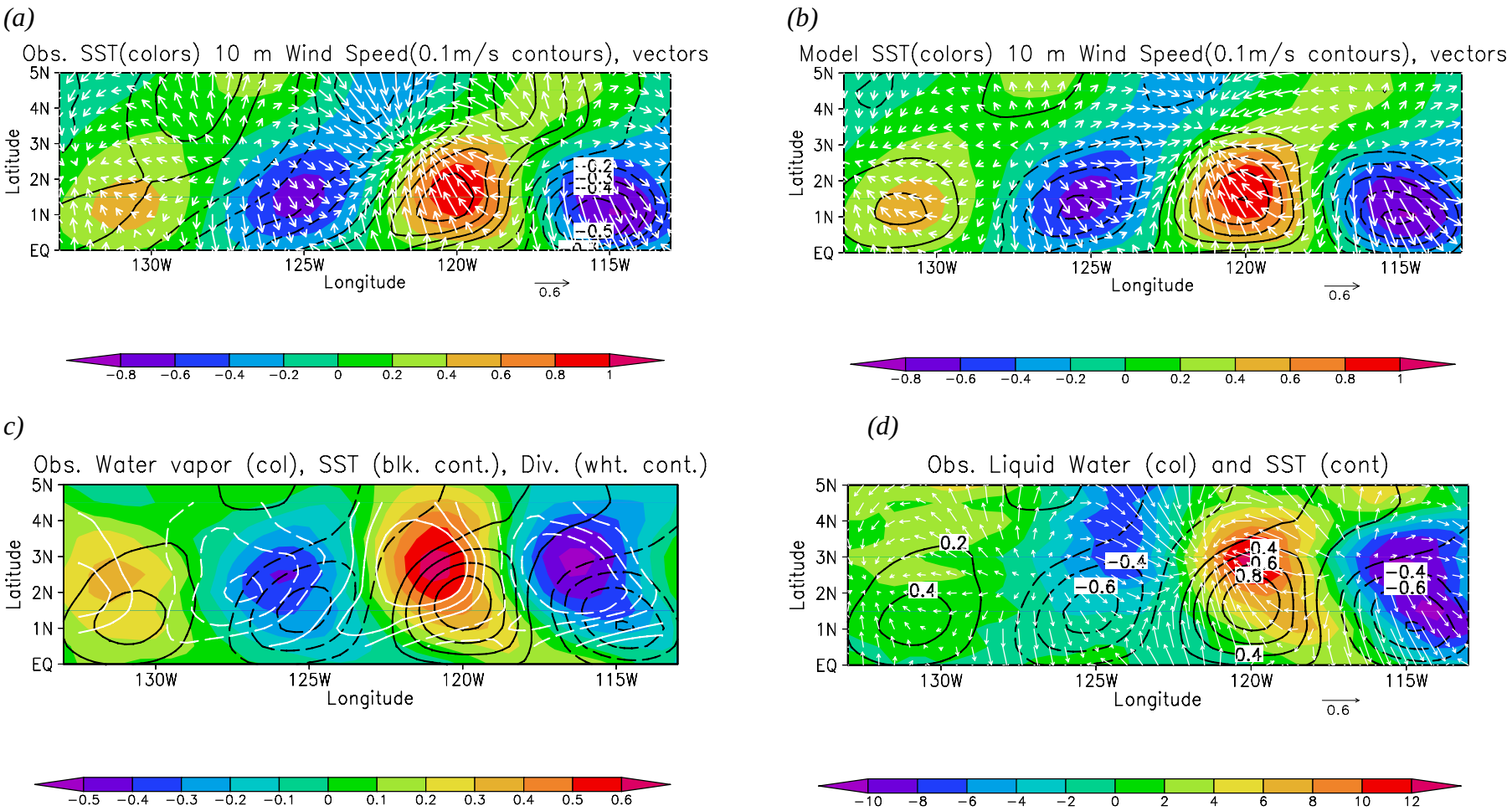

Figure 5. Composite regression onto SST at a center point of 120° W, 2° N. a) Observed SST (color) and wind velocity ($ms^{-1}K^{-1}$, see scale arrow) and wind speed($ms^{-1}K^{-1}$, contours, 0.1 $ms^{-1}K^{-1}$,interval), b) Model wind velocity ($ms^{-1}K^{-1}$, see scale arrow) and wind speed($ms^{-1}K^{-1}$, contours, 0.1 $ms^{-1}K^{-1}$,interval) forced by observed SST (color) at the surface, c) Water vapor (color, mmK^{-1}), SST (black contoured at 0.1 intervals) and wind convergence ($s^{-1}K^{-1}$, white contours, contoured for +/- 1,2,3x10^{-6} $s^{-1}K^{-1}$), d) cloud liquid water (color, $10^{-3}mmK^{-1}$) and SST (contoured at 0.1 intervals). Adapted from Small et al (2003) with permission of the American Meteorological Society.

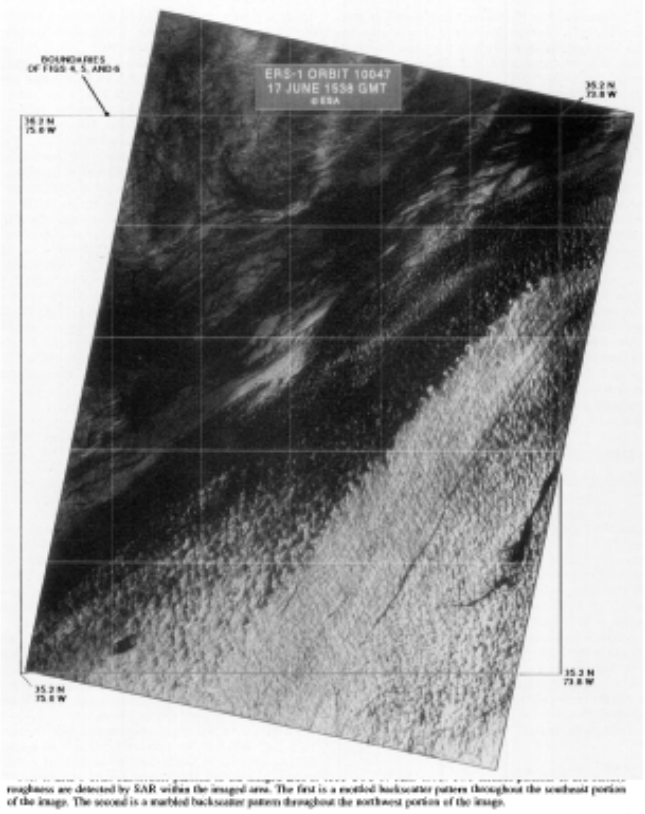

roughness are detected by SAR within the imaged area. The first is a mottled backscatter pattern throughout the southeast portion of the image. The second is a marbled backscatter pattern throughout the northwest portion of the image.

Fig. 6. a) Photograph taken from the NOAA P-3 aircraft looking northeast across the north wall of the Gulf Stream. The winds were blowing from the northeast at the time of the photograph. The seas were calm over the colder waters to the northwest of the Gulf Stream (upper left) and white caps covered the warmer water to the southeast. (Courtesy of P. Chang and D. Chelton). From Chelton et al (2006). Reproduced by permission of the American Meteorological Society. B) SAR image showing convective cells over Gulf Stream water (bottom right): smooth waters over cool shelf water (top left). From Sikora et al 1995. Reproduced by permission of the American Meteorological Society.

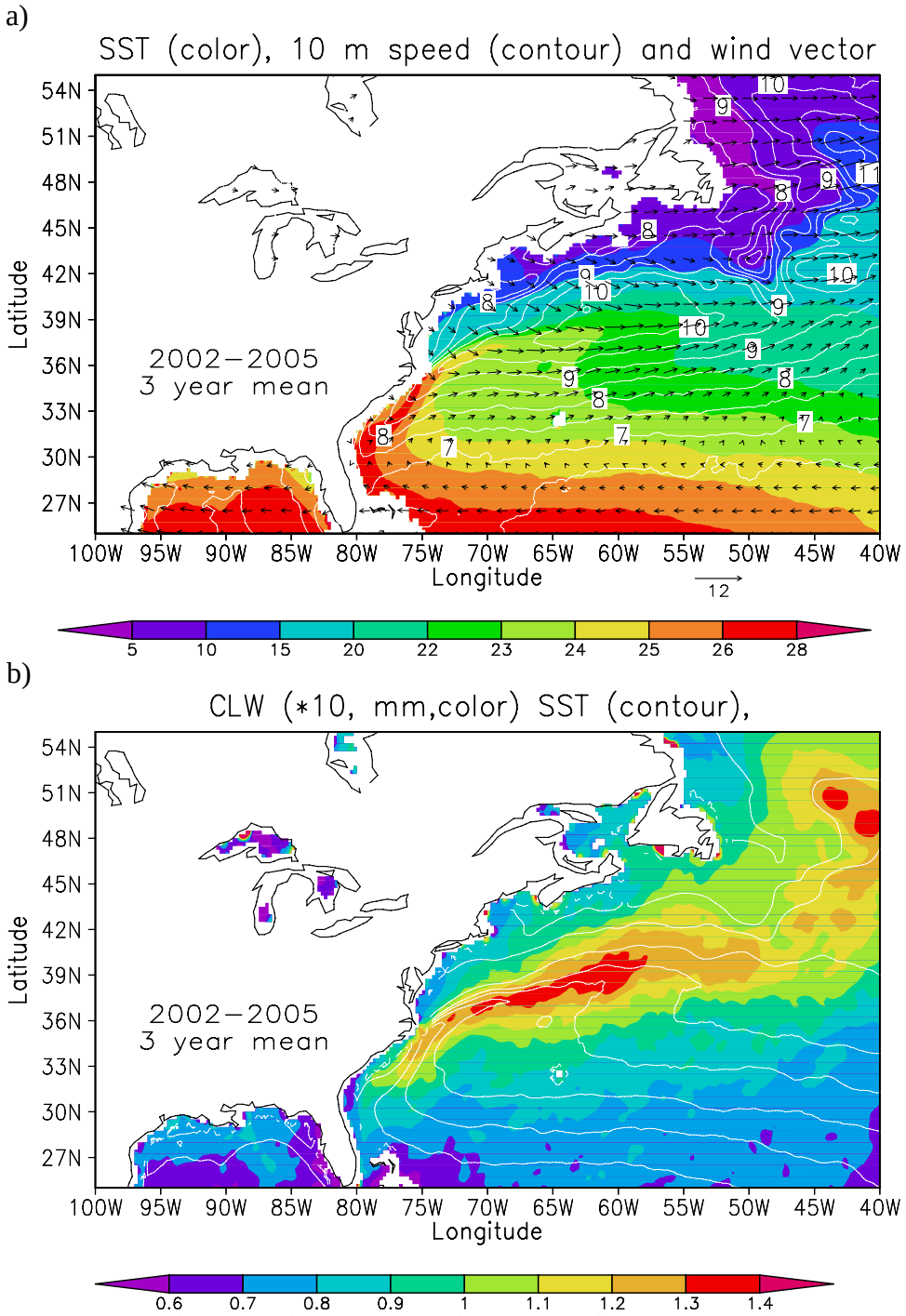

Figure 7a. North-west Atlantic SST (color, °C) and mean neutral 10 m wind speed (ms^{-1}, 1 ms^{-1} contour interval), and vectors (see scale at bottom right). A 3 year mean from June 2002 to June 2005. SST from AMSR-E and winds from QuiKSCAT. B) column integrated cloud liquid water (10^{-1} mm, color) and SST (contours at 3°C intervals). A 3 year mean from June 2002 to June 2005 from AMSR-E.

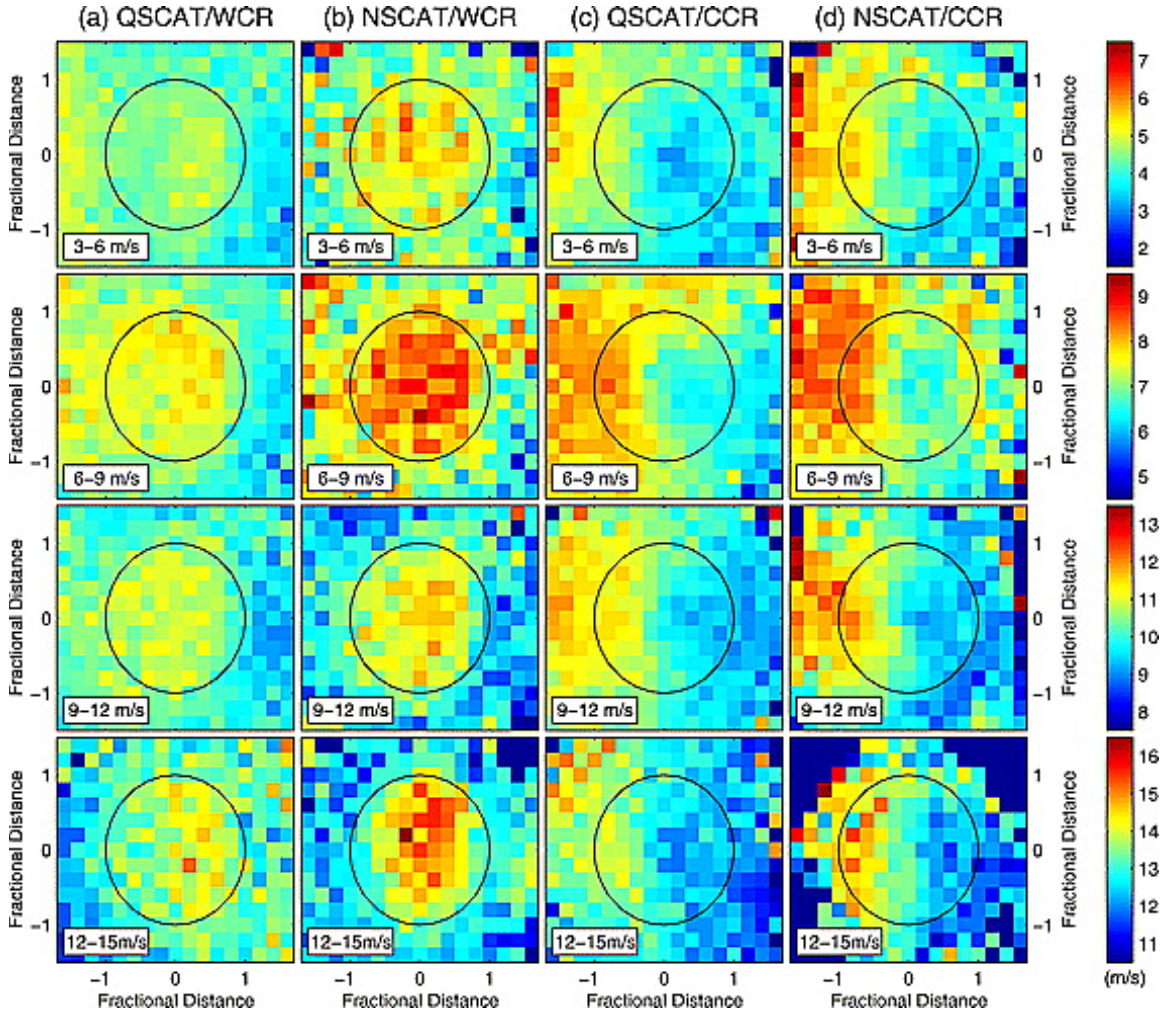

Figure 8. Gulf Stream rings. Component of scatterometer winds along the mean wind direction, in ring-centric coordinates rotated such that the mean wind is towards the top of the figure. Data are binned by mean wind speed, data set, and type of ring and averaged over all rings. A) warm core rings from QSCAT, b) warm core rings from NSCAT, c) cold core rings from QSCAT, d) cold core rings from NSCAT. From Park et al (2006). Copyright American Geophysical Union (2006) and reproduced by their permission.